View metadata, citation and similar papers at core.ac.uk

brought to you by CORE

provided by Elsevier - Publisher Connector

Cell, Vol. 109, 243–255, April 19, 2002, Copyright ©2002 by Cell Press

Representation of the Glomerular Olfactory Map in the *Drosophila* Brain

Elizabeth C. Marin,[1,4] Gregory S.X.E. Jefferis,[1,2,3,4] Takaki Komiyama,[1,2] Haitao Zhu,[1] and Liqun Luo[1,2,3]

[1]Department of Biological Sciences
[2]Neurosciences Program
Stanford University
Stanford, California 94305

Summary

We explored how the odor map in the *Drosophila* antennal lobe is represented in higher olfactory centers, the mushroom body and lateral horn. Systematic single-cell tracing of projection neurons (PNs) that send dendrites to specific glomeruli in the antennal lobe revealed their stereotypical axon branching patterns and terminal fields in the lateral horn. PNs with similar axon terminal fields tend to receive input from neighboring glomeruli. The glomerular classes of individual PNs could be accurately predicted based solely on their axon projection patterns. The sum of these patterns defines an "axon map" in higher olfactory centers reflecting which olfactory receptors provide input. This map is characterized by spatial convergence and divergence of PN axons, allowing integration of olfactory information.

Introduction

Our perception of the external world relies on two important organizational principles of the nervous system. First, the sensory world is internally represented in the brain as neural maps. In the case of the somatosensory topographic map, for example, neurons in neighboring regions of the primary somatosensory cortex respond selectively to stimulation of neighboring body parts (Penfield and Rasmussen, 1950), maintaining a somatotopy even though these cortical neurons are several synapses away from the sensory neurons. Second, neurons at different levels along central pathways must both represent and integrate sensory inputs in order to extract useful information. For instance, neurons at different levels in the central visual pathways respond to increasingly more abstract visual features, presumably by integrating information from multiple neurons early in the pathway (Hubel and Wiesel, 1962). Integration also occurs across sensory modalities, as is the case for optic tectum neurons that integrate separate maps for vision and hearing (Knudsen and Brainard, 1995). Deciphering the neuroanatomical logic of how sensory information in neural maps is relayed and integrated along central pathways will contribute to our general understanding of both organizational principles.

The olfactory system provides a useful and somewhat distinct opportunity to study the anatomical basis of neural map transfer and transformation. In other sensory maps there is a clear organization within the brain along continuous axes, for example, in the visual system reflecting the photoreceptor array of the eye. In contrast, in the olfactory system, the peripheral sense organs show little spatial order, and the first map in the central nervous system is organized very differently, in a discontinuous, punctate map (Axel, 1995; Hildebrand and Shepherd, 1997). In both mice and *Drosophila*, each olfactory receptor neuron (ORN) likely expresses only one specific odorant receptor, and cell bodies of ORNs expressing a given receptor are dispersed in the olfactory epithelia (Ressler et al., 1993; Vassar et al., 1993; Chess et al., 1994; Clyne et al., 1999; Vosshall et al., 1999, 2000). However, ORNs expressing the same odorant receptors have convergent axonal projections to specific glomerular targets in the antennal lobe/olfactory bulb, creating an odor map in this first olfactory structure of the central nervous system (Ressler et al., 1994; Vassar et al., 1994; Mombaerts et al., 1996; Wang et al., 1998; Gao et al., 2000; Vosshall et al., 2000). Indeed, imaging studies from insects and mammals have demonstrated that specific odorants elicit activation of specific sets of glomeruli in the antennal lobe/olfactory bulb (e.g., Rodrigues, 1988; Friedrich and Korsching, 1997; Galizia et al., 1999; Rubin and Katz, 1999; Belluscio and Katz, 2001). Thus, there is a glomerular code in the antennal lobe/olfactory bulb—activation of specific subsets of glomeruli—that represents the specific olfactory information the animal receives. How do higher olfactory centers read this glomerular code?

Olfactory information leaves the antennal lobe/olfactory bulb via projection neurons (PNs) in insects and mitral cells in vertebrates. These neurons send their dendrites to glomeruli, where they synapse with ORN axons, and project their axons to the mushroom body and the lateral horn of the protocerebrum in insects and to the olfactory cortex in vertebrates. We have recently shown that the glomerular targets of PNs in the antennal lobe—and hence the olfactory information they carry—are prespecified by PN lineage and birth order (Jefferis et al., 2001). Having collected information in this stereotyped fashion, how do PNs then carry it to higher olfactory centers? At one extreme, axons of PNs representing a given glomerulus (hereafter referred to as glomerular class) could connect with a specific set of third-order neurons, thus recreating a similar odor map one synapse further from the antennal lobe. It is also possible that there is extensive convergence (PNs of different glomerular classes projecting to common targets) and/or divergence (PNs of the same glomerular class projecting to different targets) such that a spatial map is no longer anatomically discernable, even if connections retain a certain degree of specificity. At the other extreme, it may not even be necessary for PNs to have an axon map in higher centers. For instance, physiological studies in locust have suggested that olfactory information is contained in individual PNs' slow temporal response

[3]Correspondence: lluo@stanford.edu (L.L.), jefferis@stanford.edu (G.S.X.E.J.)

[4]These authors contributed equally to this study.

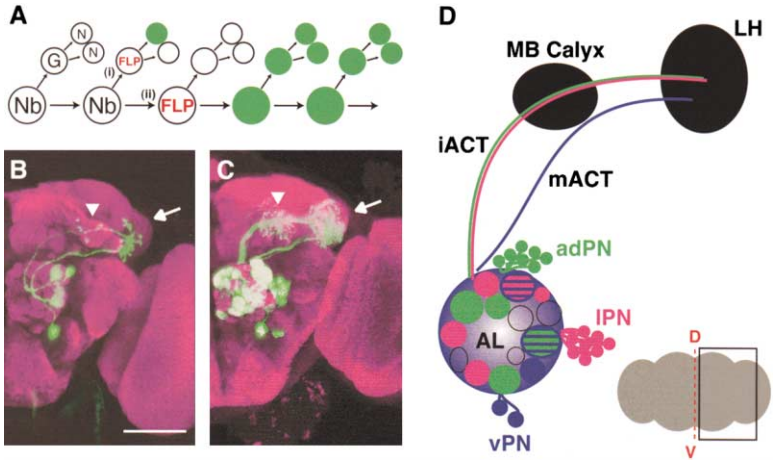

Figure 1. Projection Neuron Axon Pathways

(A) The MARCM method results in the positive labeling of a single-cell clone (i) or a neuroblast clone (ii) in the *Drosophila* central nervous system after FLP/FRT-induced mitotic recombination (Lee and Luo, 1999). Abbreviations: Nb, neuroblast; G, ganglion mother cell; N, (postmitotic) neuron.

(B and C) Composite confocal images of (B) a lateral and a ventral single-cell clone in the same brain hemisphere and (C) a lateral and a ventral neuroblast clone in the same brain hemisphere. Arrowheads indicate mushroom body calyx; arrows indicate lateral horn. The scale bar equals 50 μm. The area in the brain where the confocal images were taken is illustrated in the box on the gray brain icon in (D).

(D) A schematic summarizing the projection patterns of PNs deriving from the three major neuroblasts. Abbreviations: AL, antennal lobe; adPN, lPN, and vPN, PNs derived from anterodorsal, lateral, and ventral neuroblasts, respectively; iACT, inner antennocerebral tract; mACT, medial antennocerebral tract; MB, mushroom body; LH, lateral horn; D, dorsal, V, ventral; red dashed line, midline.

In this and all subsequent images, anterior views of the right brain hemisphere are shown with dorsal up, unless otherwise mentioned.

patterns as well as in fast temporal correlations among them (Laurent et al., 2001).

To explore this problem in *Drosophila*, we have used a genetic mosaic marking system (Lee and Luo, 1999) to examine labeled single projection neurons in hundreds of brains. We found that PNs of different glomerular classes have stereotypical axonal branching patterns in their target areas. Of ten classes of PNs that have been subjected to discriminant analysis, we can accurately predict the glomerular targets of individual PNs based on variables derived only from morphological measurements of their axonal projections. Moreover, the terminal fields of PN axons in the lateral horn are stereotyped according to PN class, yet exhibit both convergence and divergence in their projections, allowing integration of olfactory information. Using a slightly different method, Richard Axel and his colleagues have made similar observations (see Wong et al., 2002 [this issue of *Cell*]). Interestingly, we also found that PN classes with similar axon terminal fields in the lateral horn tend to receive input from neighboring glomeruli. The coupling of genetically prespecified glomerular choice of projection neurons with their stereotyped axon map provides a mechanism to organize the segregation of different olfactory information and potentially to hardwire the central olfactory system in a manner which may subserve innate odor-induced behaviors.

Results

Projection Neuron Axon Pathways

In *Drosophila*, about 1300 olfactory receptor neurons expressing 40–50 different olfactory receptors project their axons to 40–50 glomeruli in the antennal lobe (reviewed in Jefferis et al., 2002). An estimated 150–200 antennal lobe projection neurons send dendrites to these glomeruli and axons to the mushroom body and the lateral horn of the protocerebrum (Stocker et al., 1990, 1994; Laissue et al., 1999; Jefferis et al., 2001). The MARCM (mosaic analysis with a repressible cell marker) method (Lee and Luo, 1999) allows us to generate uniquely labeled neuroblast and single-cell clones in the *Drosophila* central nervous system (Figure 1A). We selectively visualized antennal lobe projection neurons (PNs) by using the driver *GAL4-GH146* (Stocker et al., 1997), which labels ~50 adPNs derived from the anterodorsal neuroblast, ~35 lPNs derived from the lateral neuroblast, and 6 vPNs derived from the ventral neuroblast, occupying ~30 glomeruli (Jefferis et al., 2001; this study; Wong et al., 2002). When we perform MARCM using *GAL4-GH146*, we can label single-cell (Figure 1B) or neuroblast (Figure 1C) clones of PNs that allow us to determine their glomerular targets in the antennal lobe and their axon projection pathways and termination patterns in the mushroom body and lateral horn.

Our initial findings are consistent with earlier Golgi staining and tracer injection results in *Drosophila* and other insects (e.g., Stocker et al., 1990; Homberg et al., 1989; Malun et al., 1993) and are summarized in a schematic (Figure 1D). PNs arising from the anterodorsal and lateral neuroblasts project their axons via the inner antennocerebral tract (iACT) that passes through the anterior aspect of the mushroom body calyx, where they send collaterals to synapse with dendrites of mushroom body neurons. These PN axons eventually terminate in the neuropil of the lateral horn. By contrast, the axons of PNs from the ventral neuroblast travel to the lateral horn via the medial antennocerebral tract (mACT) that bypasses the mushroom body calyx altogether. Although the uniglomerular dendritic projections of the anterodorsal and lateral PNs are distinct and nonoverlapping (Jefferis et al., 2001), two glomeruli in the antennal lobe are innervated by both ventral and either anterodorsal or lateral PNs (Figure 1D; see below).

Stereotypical Axon Terminals in Neuroblast Clones

We first noticed that axon terminals from the three types of neuroblast clones are characteristic and readily distinguishable from one another in two-dimensional (2D) projections of confocal stacks. Axons from anterodorsal neuroblast clones (Figure $2A_0$) occupy a small portion of the mushroom body calyx near the dorsoventral axis and the ventral half of the lateral horn with only a few, distinctive, dorsal branches (Figure $2A_{1-3}$). By contrast, axons from lateral neuroblast clones (Figure $2B_0$) ramify

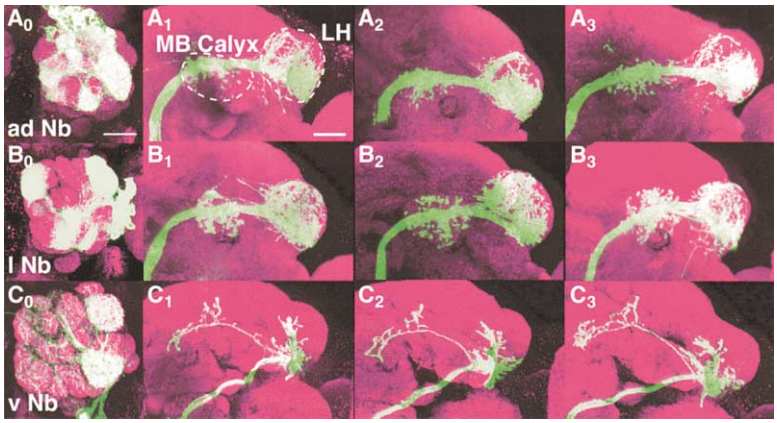

Figure 2. Stereotypical Axon Terminals in Neuroblast Clones

(A_{0-3}) A typical anterodorsal neuroblast clone in the antennal lobe (A_0) and typical axon projection patterns from three individual animals (A_{1-3}). The scale bars equal 20 μm.
(B_{0-3}) A typical lateral neuroblast clone in the antennal lobe (B_0) and typical axon projection patterns from three individual animals (B_{1-3}).
(C_{0-3}) A typical ventral neuroblast clone in the antennal lobe (C_0) and typical axon projection patterns from three individual animals (C_{1-3}).
Abbreviations: ad, anterodorsal; l, lateral; v, ventral; Nb, neuroblast; MB, mushroom body; LH, lateral horn. Clones were generated from early heat shock-induced recombination and include PNs innervating all landmark glomeruli seen in the full GH146 expression pattern for each neuroblast type. All images are 2D maximum intensity Z projections of confocal stacks.

more broadly in both the mushroom body calyx and the lateral horn (Figure 2B_{1-3}), despite the fact that they derive from about 15 fewer PNs. Axonal projections of ventral neuroblast clones (Figure 2C_0) are most distinctive, as they appear to project to a more anterior and ventral region of the lateral horn than those of anterodorsal or lateral neurons and to include a highly stereotypical branch that runs anteriorly and parallel to the dorsal edge of the brain toward the midline (Figure 2C_{1-3}). Since adPNs and lPNs innervate different subsets of glomeruli (Figure 1D; Jefferis et al., 2001) and therefore carry different sets of olfactory information, these observations provide the first indication of spatial segregation of olfactory information in the mushroom body and lateral horn.

Stereotypical Axon Branching Patterns and Terminal Fields in Single-Cell Clones

We next tested whether PNs of different glomerular classes exhibit distinct axon projection patterns at the single-cell level. We found that PNs innervating particular glomeruli in the antennal lobe exhibit stereotypical axon branching patterns in the lateral horn that can be readily observed in 2D confocal stacks (Figures 3A–3H). For instance, the axons of all DL1 neurons examined ($n > 100$) display a major dorsal branch as they enter the lateral horn, such that there are two distinct areas of termination (Figure 3A). Axons of DL3 neurons also exhibit a major dorsal branch, but it emerges further inside the lateral horn (Figure 3G). In contrast, the axons of all VA1d neurons have a more restricted innervation region in the center of the lateral horn (Figure 3B), while those of 1 and VM2 neurons show relatively simple patterns (Figures 3C and 3F). Axon patterns in the mushroom body calyx appear much less stereotypical (Figures 3A–3H).

Analysis of the axons of PNs arising from the ventral neuroblast revealed several noteworthy features. Both lateral and ventral PNs innervate glomerulus DA1, while both anterodorsal and ventral PNs innervate glomerulus VA1lm. In both cases, the two cell types innervating the same glomerulus have different axon branching patterns and spatial locations in the lateral horn, implying two different representations in this higher olfactory center for the activation of each of these two glomeruli. Lateral PNs innervating all (Figure 4A) or part (Figure 4B) of DA1 exhibit fairly simple axon patterns confined to the ventral half of the lateral horn, while anterodorsal PNs innervating VA1lm (Figure 4D) exhibit a highly distinctive axon branching pattern in the central and ventral regions of the lateral horn. The axon patterns of ventral PNs innervating DA1 (Figure 4C) and VA1lm (Figures 4E and 4F) are quite similar to each other and much more complex than their anterodorsal or lateral counterparts. In contrast, a ventral PN uniquely innervating VL1 exhibits a distinctive, diffuse, and highly complex axon pattern along the ventral border of the lateral horn (Figure 4G). Lastly, there is a ventral PN whose dendrites ramify throughout much of the antennal lobe (though notably not VL1). It sends its axon branch anteriorly from the ventral lateral horn toward the midline of the brain (Figure 4H), transferring information to unidentified additional brain centers.

Additional Spatial Organization of Axon Branching Pattern Revealed by 3D Reconstruction

We next created three-dimensional (3D) reconstructions of PN axons from 2D confocal stacks using the axon tracing software Neurolucida in order to analyze these data quantitatively and with higher resolution (Figure 5A). We also traced the contours of the lateral horn area innervated by PNs using the nc82 counterstaining (which labels all synaptic regions in the *Drosophila* brain) as a guide. This allowed us to compare the spatial distribution of PN axons from different brains.

Three-dimensional reconstruction revealed differences in PN axon projection patterns that were not apparent in 2D confocal stacks. For example, DA1 neurons from the lateral neuroblast appear to innervate the center of the lateral horn in 2D stacks (Figures 4A and 4B). However, dorsal and lateral views of these neurons revealed that they actually innervate a strikingly small area at the very anterior edge of the lateral horn (Figure 5B2). This approach also allowed us to distinguish some PN classes whose 2D projection patterns appear relatively similar. For example, VA1d and VA1lm PNs from the

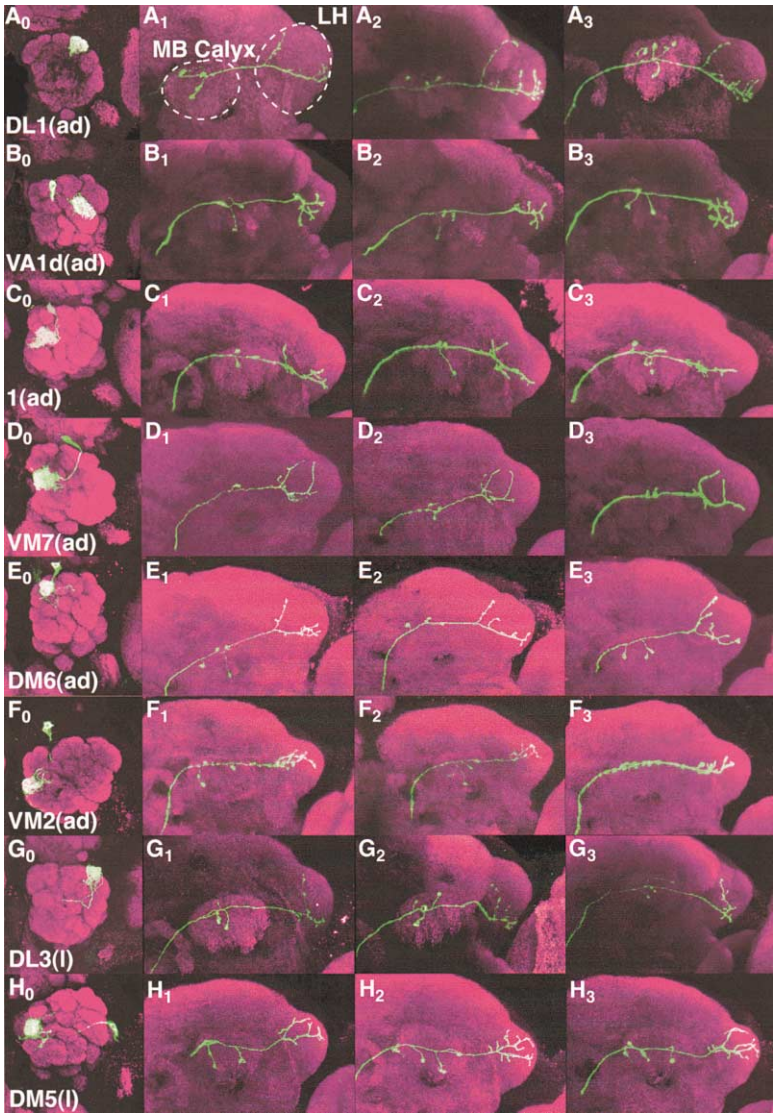

Figure 3. Stereotypical Axon Branching Patterns in Single-Cell Clones

(A_0–H_0) Typical examples of the antennal lobe glomerular innervation patterns of eight PN classes, six anterodorsal and two lateral.

(A_{1-3}–H_{1-3}) Axon projection patterns from three individual animals for each of the eight PN classes.

Parentheses indicate neuroblast of origin. Abbreviations: ad, anterodorsal; l, lateral; MB, mushroom body; LH, lateral horn. All images are 2D maximum intensity Z projections of confocal stacks.

anterodorsal neuroblast both appear to innervate roughly the ventral half of the lateral horn when observed in 2D stacks (Figures 3B and 4D). However, observation of dorsal and lateral views (Figure 5B3) revealed that the innervation of VA1d PNs is restricted to the anterior part of the lateral horn, while VA1lm PNs have a much more widely distributed innervation area along the A-P axis (Figure 5B4).

Quantitative Analysis of Axon Branching Patterns

The qualitative differences in axon branching patterns we have described so far are quite striking. Our observations suggest that projection neurons of different glomerular classes have distinct overall 3D axon branching patterns as well as overlapping but distinct innervation areas in lateral horn. To explore this hypothesis further, we ask the following questions: First, can the stereotypy of axon branching patterns be demonstrated quantitatively? Second, is there a spatial order in the axon terminal field? Third, do different PN classes have overlapping axon terminal fields? Lastly, is there any discernable logic governing which PN classes have similar axon terminal fields?

We focused our further analysis on 11 classes of adPNs and lPNs, as we were able to obtain 13–16 high-quality single-cell clones for each class. We took the 3D reconstruction data from these 161 PNs and measured a number of different morphological properties of the axons. Operationally, these properties fall into two groups that we term branching variables and spatial variables. Branching variables are those calculated using only the reconstructed axon, such as the total length of the axonal tree in the lateral horn or the number of collateral branches in the mushroom body. Spatial variables are those which indicate the location of different parts of the axon with respect to the animal's brain and are calculated using both the reconstructed axon and the contours which define the lateral horn area. Examples include the 3D location of the mean of the lateral horn axon terminal endpoints. We initially calculated measurements for 37 such variables from the neurons in our data set; this number was subsequently

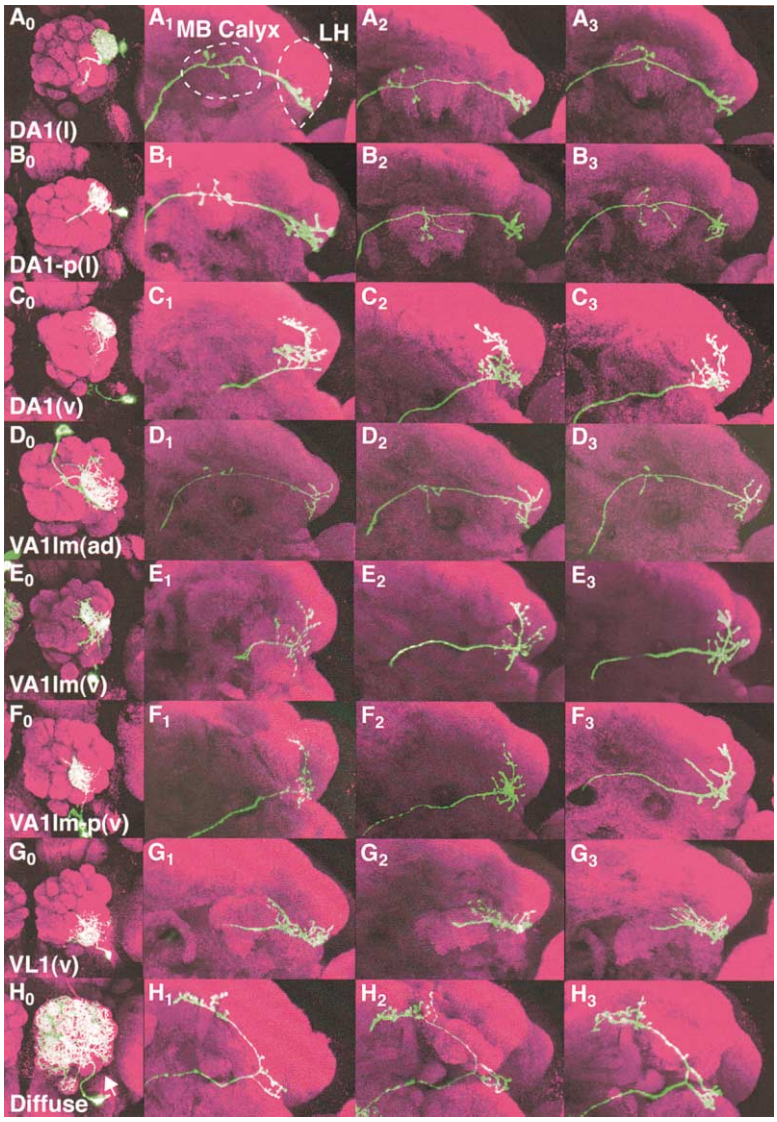

Figure 4. Stereotypical Axon Branching Patterns in Single-Cell Clones: Special Cases

(A_0–H_0) Typical examples of the antennal lobe glomerular innervation patterns of eight PN classes: two lateral, one anterodorsal, and five ventral.

(A_{1-3}–H_{1-3}) Axon projection patterns from three different animals for each of the eight PN classes.

Parentheses indicate neuroblast of origin. Arrow indicates noninnervated VL1 in H_0. Abbreviations: ad, anterodorsal; l, lateral; v, ventral; p, partial; MB, mushroom body; LH, lateral horn. All images are 2D maximum intensity Z projections of confocal stacks.

reduced to 15 selected variables (Figure 6 legend) by eliminating those variables that did not provide useful information (for more details, see Experimental Procedures and Supplemental Data at http://www.cell.com/cgi/contenct/full/109/2/243/DC1).

We applied the statistical technique known as linear discriminant analysis (LDA) to investigate whether different classes of PN have distinct axon projection patterns. This technique takes as its input a set of data in which individual PNs are described by several variables and have a class label; it produces a set of discriminant functions, which are weighted combinations of the input variables that best separate the individuals into their assigned classes. We then used a crossvalidation procedure summarized in Figure 6A to examine whether the PN classes could be reliably distinguished. (1) We took the available morphological data and split it randomly into a large *training set* and a small *test set*. The training set neurons retained their PN class labels; in the test set these labels were temporarily set aside. (2) We used the training set neurons to train the linear discriminant functions [black box, ? → f(x)]. (3) Next, we produced *predicted class labels* for the test neurons (that had in no way contributed to training of the discriminant functions) by passing the values of their axonal variables as input to the discriminant functions. (4) Finally, we compared the predicted class labels of the test neurons with the true class labels that had earlier been set aside to calculate a *prediction error rate*. Steps 1–4 were repeated 40 times to generate an average prediction error.

The performance of LDA on our test data is summarized in the matrix shown in Figure 6B. Along the top of the table are the true class labels; along the left side, the predicted class labels. The entries of the matrix therefore correspond to the percentage of occasions on which a test set neuron of true class X (along the top) was predicted to be of class Y (along the left side). The leading diagonal thus contains the percentage of occasions on which neurons were correctly classified. After merging the DA1 and DA1-p classes, which were largely indistinguishable (see Figure 4), our final predic-

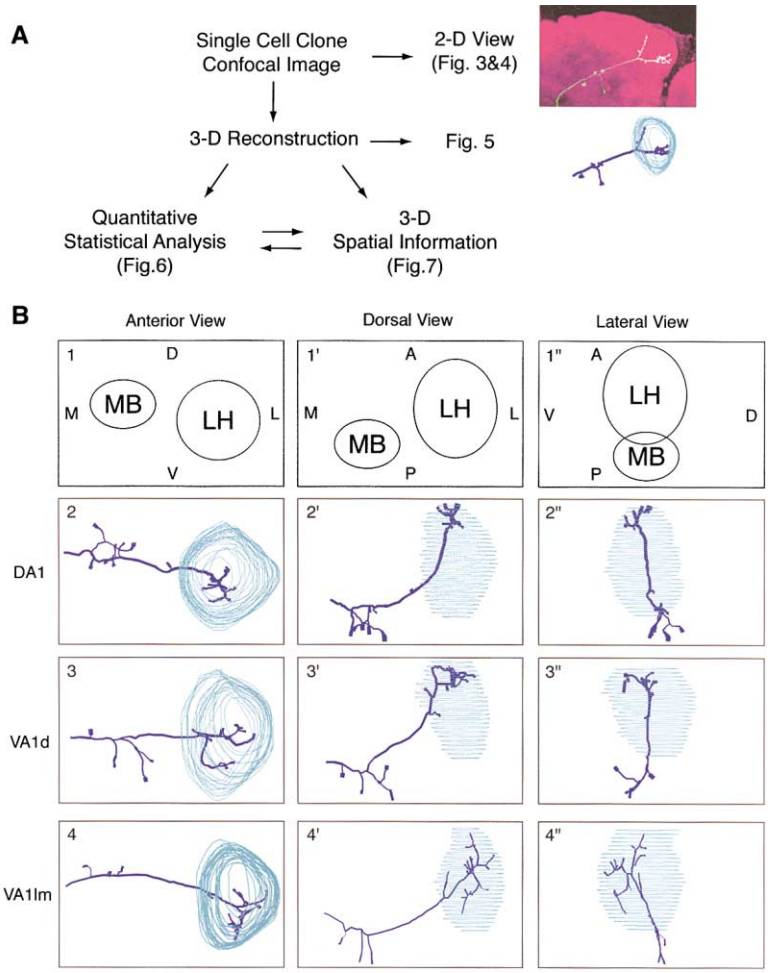

Figure 5. 3D Reconstruction of Single-Cell Clone Axon Images

(A) Flowchart of information processing described in this paper.

(B) Three examples of 3D reconstruction: anterior (2, 3, 4), dorsal (2′, 3′, 4′), and lateral (2′′, 3′′, 4′′) views of a DA1 neuron from the lateral neuroblast (2, 2′, 2′′) and of a VA1d neuron (3, 3′, 3′′) and a VA1lm neuron (4, 4′, 4′′) from the dorsal neuroblast. Blue indicates axon, light blue indicates contours of lateral horn. The numbers 1, 1′, and 1′′ schematize the approximate positions of lateral horn and mushroom body and the orientation (Abbreviations: P, posterior; A, anterior; D, dorsal; V, ventral; L, lateral; M, medial) from each view.

tion error was 7.8% ± 0.1% (Figure 6B; for further details, see Supplemental Data at http://www.cell.com/cgi/contenct/full/109/2/243/DC1). Since we now had ten PN classes, random classification by LDA would have resulted in an approximately 90% prediction error. The fact that we can predict, with minimal error, the glomerular identity of PNs based simply on these axonal variables demonstrates the highly stereotyped organization of the axonal projection patterns of PNs.

Discriminant analysis also allowed us to determine which morphological properties of axons contributed most to distinguishing different classes of PNs. To determine the relative "importance" of each of the 15 variables, we removed each variable in turn from the data set and determined the increase in the prediction error rate in the absence of the removed variable. Figure 6C shows the results of such analysis. As can be seen, the variables *SDy*, *Dx*, and *Dz* are the most significant, as removal of these variables individually caused the greatest increase in prediction error rates. Interestingly, all three are spatial variables relating to the position of axons in the lateral horn (see Figure 6 legend). Thus, it appeared that PNs of different classes are best distinguished by the spatial location of their axon terminal endpoints in the lateral horn, so we next examined the spatial organization of PN axons in the lateral horn.

Spatial Order in the Lateral Horn

By uniformly scaling all lateral horn outlines (see Experimental Procedures), we were able to superimpose the axon termination patterns of many PNs onto a standard lateral horn. As was evident from the raw 3D reconstruction data, these patterns were spatially distinct for different PN classes. To test statistically whether the axons of different PN classes terminate in spatially stereotyped locations in the lateral horn, we initially simplified our data set as follows. We reasoned that if PN endpoints are stereotyped, then the mean position (or centroid) of the endpoints for each individual PN should also be spatially stereotyped. We calculated the mean axon endpoint positions for all 161 neurons and plotted them in a standard brain (Figure 7A). These mean axon endpoint positions are clearly clustered for different classes of PN. We carried out a permutation test to assess the significance of this clustering: a clustering index was calculated for our data and compared with the distribution of clustering indices calculated after randomly permuting the class labels of the 161 data points, thereby simulating an absence of spatial order (see Experimental Procedures for details). This demonstrated that the observed spatial clustering of PNs of the same class was statistically significant, with $p < 0.0005$ (Figure 7B).

While the above permutation test provides convincing

A

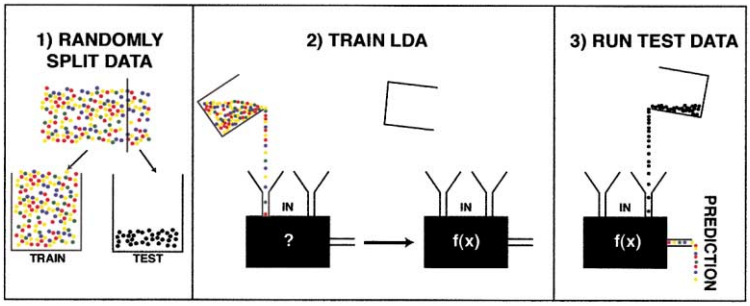

B

	true									
predicted	1	DA1	DL1	DL3	DM5	DM6	VA1d	VA1lm	VM2	VM7
1	90.3	0.2	0.0	0.0	0.0	0.0	0.2	0.0	0.0	4.2
DA1	0.0	93.4	0.0	4.6	0.0	0.0	2.8	0.0	0.0	0.0
DL1	0.0	0.0	88.6	0.2	0.0	1.3	0.0	0.0	0.0	0.0
DL3	0.0		0.0	83.4	0.0	0.0	0.0	0.0	0.0	0.0
DM5	0.0	0.0	0.0	0.0	96.9	0.0	0.0	0.0	0.8	0.0
DM6	0.0	0.0	12.3	0.0	0.0	97.9	0.0	0.0	0.0	4.7
VA1d	0.0	5.7	0.0	1.8	0.0	0.0	89.0	0.0	0.0	6.7
VA1lm	0.0	0.0	0.0	6.7	0.0	0.0	6.2	100.0	0.0	0.0
VM2	0.0	0.0	0.0	0.0	2.5	0.0	0.0	0.0	99.1	0.0
VM7	10.2	0.0	0.0	0.0	0.7	0.7	0.0	0.0	0.0	84.0

C

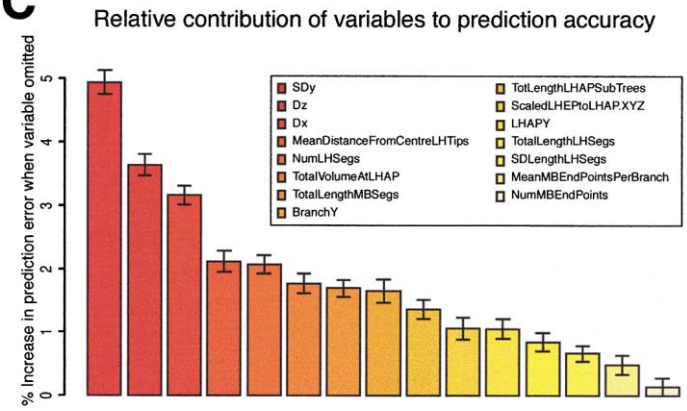

Figure 6. Linear Discriminant Analysis (LDA)

(A) Schematic illustrating linear discriminant analysis and crossvalidation procedure.

(B) Summary of predictions: results of LDA using 15 most useful variables and with DA1 and DA1-p merged into one class. Green (leading diagonal) indicates percentage of correct classifications; red indicates percentage of prediction errors. See text for details.

(C) Contribution of the 15 different selected variables to the discrimination process. Definitions of variables used are as follows: SDy, standard deviation of the axon terminal positions along the dorsoventral axis; the maximum extent of the standard lateral horn along each axis corresponds to ±1 unit (hereafter, standard lateral horn coordinates); Dx and Dz, mean position of a neuron's axon endpoints along the mediolateral and anteroposterior axes in standard lateral horn coordinates; MeanDistanceFromCentreLHTips, average 3D distance in microns from a neuron's axon endpoints in the lateral horn to the centroid of those axon endpoints—i.e., a measure of how spread-out the endpoints are; NumLHSegs, number of branch segments in the lateral horn; TotalVolumeAtLHAP, volume of the convex hull enclosing the branches distal to the major branch point in the lateral horn measured in cubic microns; TotalLengthMBSegs, total length of the collateral branches in the mushroom body; BranchY, mean position along the dorsoventral axis of the whole of the axonal tree in standard lateral horn coordinates; TotLengthLHAPSubTrees, length in microns of the subtrees distal to the major branch point in the lateral horn; ScaledLHEPtoLHAP.XYZ, 3D distance from the entrance to the major branchpoint in the lateral horn in standard lateral horn coordinates; LHAPY, dorsoventral position of the major branchpoint in standard lateral horn coordinates; TotalLengthLHSegs, total length in microns of the axonal tree in the lateral horn; SDLengthLHSegs, standard deviation in microns of the length of every segment of the axonal tree in the lateral horn; MeanMBEndPointsPerBranch, number of endpoints (likely to be the only synapses) per collateral branch in the mushroom body; NumMBEndPoints, total number of endpoints in the mushroom body calyx.

evidence that projection neurons have spatially ordered terminations in the lateral horn, it does not provide information as to the precise arrangement of axon terminal fields. We therefore plotted all axon terminal endpoints of any particular PN class (average 11.2 ± 0.3 per neuron) and asked whether the endpoints of different PN classes occupy similar or different regions in space. In Figures 7C–7F each stereo pair shows all the endpoints belonging to two different classes of PNs in two different colors. These plots revealed important features of the PN axon terminal fields. First, while the terminal fields of some PN classes occupy a small region (notably DA1, see also Figure 5B2), most occupy a rather large volume of the lateral horn (note: the length of the axes indicates the maximum size of the standard lateral horn in a particular dimension). Thus, it would seem that a single PN class could potentially activate target neurons across a broad extent of the lateral horn.

Second, we can obtain information regarding not only the spatial termination of a particular PN class but also the relationship between different PN classes. For instance, DL1 and DM6 both exhibit prominent dorsal collateral branches (Figures 3A and 3E), and this is reflected in two major clusters in their terminal fields. When all axon endpoints for each DL1 and DM6 PN are plotted, it can be seen that DL1 and DM6 PNs terminate in very similar locations (Figure 7C). It is therefore likely that DL1 and DM6 PNs would activate largely overlapping sets of third-order neurons. However, DL1 and VA1lm terminal fields show partial overlap—only the ventral branch of DL1 overlaps with VA1lm (Figure 7D). Thus, third-order neurons innervating the ventral lateral

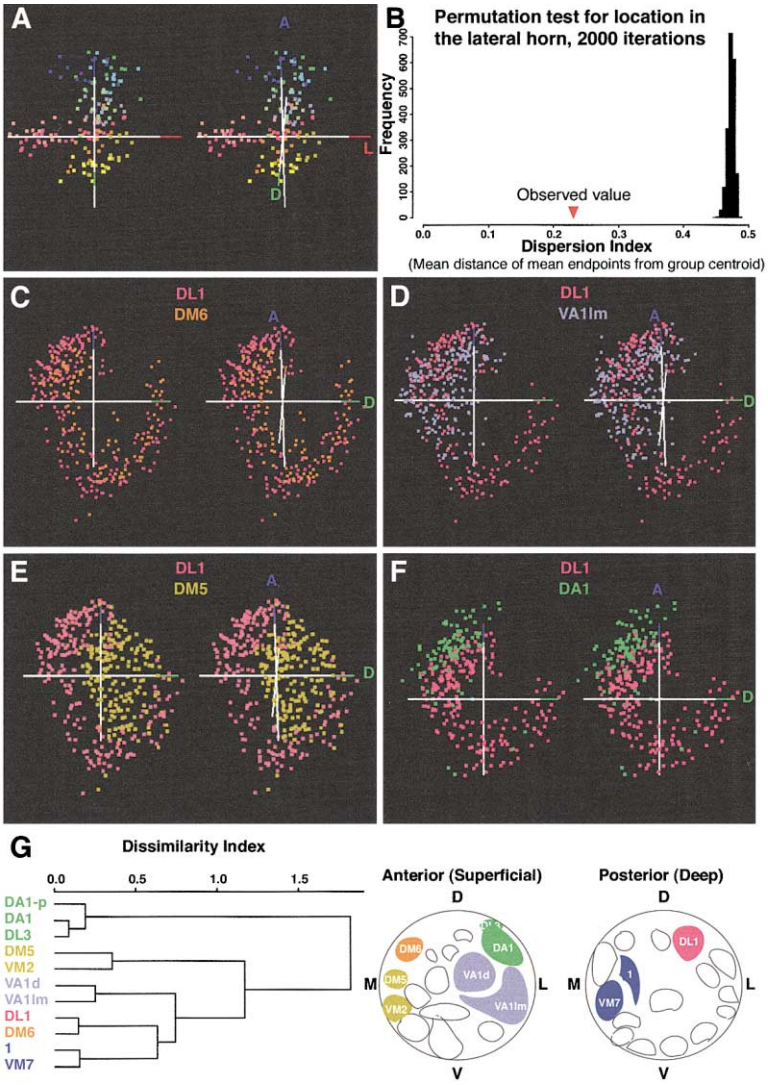

Figure 7. Spatial Order of Projection Neuron Terminal Field in the Lateral Horn

(A) A stereo pair showing the mean endpoint positions of individual PNs for all 161 PNs in a standard lateral horn which has been rotated 30° about the mediolateral axis; different colors represent different glomerular classes. Axes are ±1 unit long.

(B) Permutation test for nonrandom location of mean endpoint positions.

(C–F) Stereo pairs of DL1 class and four other classes of PNs. Axes are ±1 unit long. (C)–(E) are rotated 30° about the dorsoventral axis, while (F) is a view looking directly along the mediolateral axis.

Abbreviations: A, anterior; D, dorsal; L, lateral.

(G) Dendrogram of axon terminal field similarity for different PN classes. Horizontal distance indicates degree of axon terminal field dissimilarity. At right are diagrammed locations of the glomeruli innervated by the 11 PN classes. (Abbreviations: D, dorsal; V, ventral; M, medial; L, lateral). See text for detail.

horn could receive input from both PN classes in order to generate a response to DL1 and VA1lm activation, while third-order neurons innervating the dorsal area could sample DL1 without VA1lm. DM5 and DA1 (Figures 7E and 7F) show much less overlap with DL1—indeed, the DM5 terminal field neatly intercalates between the two major branches of DL1 (Figure 7E). This arrangement suggests that fewer third-order neurons are likely to be coactivated by DL1 in combination with either DM5 or DA1.

Lastly, quantitative analysis of the degree of overlap of axon terminal fields for every pair of PN classes allowed us to generate a distance matrix plotted as a dendrogram (Figure 7G). This dendrogram indicates the degree of similarity among different PN classes with regard to their lateral horn axon terminal fields. PN classes with axon terminal fields occupying the same part of the lateral horn with the same density of terminations would have a score of zero. Scores greater than zero indicate the degree to which the two PN classes have distinct projection patterns. The 11 classes of PNs are separated into five distinct clusters. Interestingly, four of these five clusters corresponded to a pair or triplet of adjacent or almost adjacent (VM2 and DM5) glomeruli. The one exception was the pair DL1 and DM6, which are separated by two intervening glomeruli not included in this analysis.

Early Formation of PN Axon Branches

To begin to understand the mechanisms of formation of stereotypical PN axon projections, we examined when their axon branches form during development. We focused on the DL1 class because 100% of labeled single-cell clones generated in early larvae belong to the DL1 class (Jefferis et al., 2001), allowing identification prior to glomerular formation. At 24 hr after puparium formation (APF), most DL1 axons had reached the lateral horn (data not shown). At 30 hr APF, all DL1 PNs examined had extended their main axon branch to the distal edge of the lateral horn. At least eight of the ten clones examined had also established their stereotypical dorsal branches (Figure 8A). These stereotypical dorsal branches can also be seen in neuroblast clones (Figure 8B, n = 12). At this stage, pioneering olfactory receptor

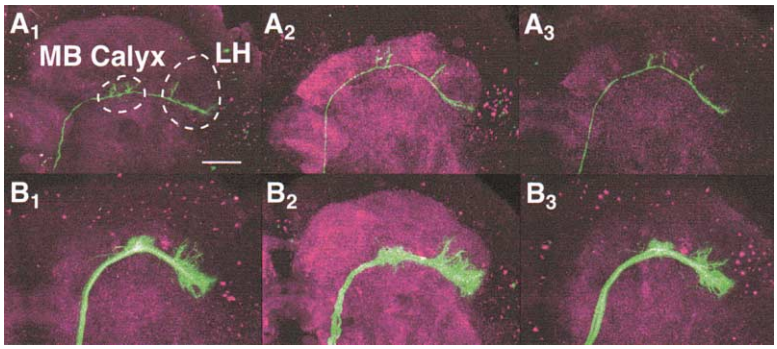

Figure 8. Early Formation of PN Axon Branches

Axon projection patterns from three DL1 PN single-cell clones (A_{1-3}) and three anterodorsal neuroblast clones (B_{1-3}) at 30 hr after puparium formation. The scale bar equals 20 μm.

axons have only arrived at the protoantennal lobe ~8 hr earlier. The formation of the first glomerulus is not visible for another 6 hr, and most glomeruli are not detectable for at least 10 hr (Jhaveri et al., 2000; our unpublished observations). Moreover, the earliest olfactory receptor expression is not detected for at least another day (Clyne et al., 1999). Thus, the gross features of the stereotypical branching pattern of DL1 PNs are most unlikely to be influenced by olfactory sensory input.

Discussion

Antennal lobe projection neurons collect olfactory information from ORN axons at specific glomeruli and then relay that information to the mushroom body and lateral horn. In this study, we have systematically analyzed the dendrite and axon projection patterns for a large subset of projection neurons with single-cell resolution. These analyses allow us to describe the general rules of how the olfactory map in the antennal lobe is represented in higher brain centers. These rules have important implications for how olfactory information is processed and how the olfactory neural network is set up.

A Stereotyped "Axon Map" for Projection Neurons in Lateral Horn

The most striking observations we made in this study are the stereotypy of the axon branching patterns and the spatial organization of their terminal fields in the lateral horn for each glomerular class of projection neuron. Much of this stereotypy can be readily discerned from the two-dimensional axon branching patterns of the different neuroblast clones (Figure 2) and single-cell clones of 16 different classes of PNs (Figures 3 and 4) and additionally from examining their axon branching patterns in three-dimensional space (Figure 5). Significantly, we could predict, with 92% accuracy, the glomerular origin of individual PNs based solely on their axon projection patterns (Figure 6B). Thus, the axon projection patterns of PNs largely maintain the information of their glomerular class, and therefore the odorant receptors that are activated (since the majority of PNs we analyzed are uniglomerular). In short, there is an anatomically discernable PN axon map.

It is important to note that exactly how this axon map is utilized will have to be elucidated by future systematic functional analysis of the third-order neurons in response to olfactory stimuli. However, our study begins to shed light on the logic of the organization of olfactory information processing beyond the antennal lobe. Although the stereotypical branching patterns in the lateral horn of individual PNs are remarkable, discriminant analysis revealed that the variables that contribute most to discriminating different PN classes are those regarding spatial distribution of axon endpoints in the lateral horn (Figure 6C). It is therefore possible that the stereotypical branching patterns of axons serve the purpose of allowing them to occupy stereotypical target areas. Indeed, a conservative statistical analysis revealed that averaged axon endpoints are distributed in a highly nonrandom fashion (Figure 7A). Compilation of all axon endpoints for given classes of PNs further reveal strikingly stereotypical organization in the lateral horn (Figures 7C–7F). Additional quantitative analysis of the spatial order of this axon map in the lateral horn allowed us to extract more information about the logic of olfactory information processing, as discussed below.

PNs with Similar Axon Terminal Fields Tend to Receive Input from Neighboring Glomeruli

We found that PNs with similar axon terminal fields tend to receive input from neighboring glomeruli (Figure 7G). The converse is not necessarily true. For instance, DM5 and DM6 PNs project to neighboring glomeruli, but their axon maps differ considerably (Figures 7C and 7E). The same applies to VA1d and DA1 (data not shown). Interestingly, in both of these cases, one PN class derives from the anterodorsal neuroblast lineage (DM6 or VA1d), and the other PN class derives from the lateral neuroblast lineage (DM5 or DA1). These observations raise an intriguing possibility that the degree of similarity of PN axon projections corresponds largely to their glomerular positions, with lineage perhaps playing a minor role. What could be the functional significance of this observation and the developmental mechanisms responsible?

Molecular genetic studies in mice have suggested that olfactory receptor neurons that exhibit a high degree of sequence similarity recognize similar odors and frequently project to adjacent glomeruli (Wang et al., 1998; Malnic et al., 1999; Tsuboi et al., 1999). Indeed, imaging studies in honeybee, zebrafish, mice, and rats have shown that structurally similar odorants tend to activate adjacent and overlapping glomeruli (Sachse et al. 1999; Friedrich and Korsching, 1997; Rubin and Katz, 1999; Uchida et al., 2000; Belluscio and Katz, 2001; Meister and Bonhoeffer, 2001). Given the striking similarity in the organization of peripheral olfactory systems in *Dro-*

sophila and mice (Vosshall et al., 2000), this "odotopy" may well hold true in *Drosophila*. If that is the case, then our observation that PNs with similar axon projection patterns tend to receive input from neighboring glomeruli would imply that the lateral horn neuropil also has an odotopic organization—similar odors likely activate similar third-order neurons. This organization may reflect the behavioral significance of different odors, connecting odors indicating proximity to food, mating pheromones, or proper sites for egg laying to distinct output neurons controlling different aspects of animal behavior.

One can also envision developmental mechanisms that could contribute to this wiring logic (similar axon patterns, adjacent glomeruli). We have recently shown that PN glomerular targets are prespecified according to lineage and birth order (Jefferis et al., 2001), likely by endowing PNs born at different times and places with different cell surface recognition molecules that allow their dendrites to be precisely targeted to specific glomeruli. If these recognition molecules are also used to specify their stereotypical axon branching pattern and terminal fields in the lateral horn, then close resemblance in the repertoire of recognition molecules that would allow different PN classes to be targeted to adjacent glomeruli may simultaneously allow their axons to be targeted to similar areas in the lateral horn. Such mechanisms could enable efficient assembly of neural networks, coordinating the input and output specificity of long-distance projection neurons with a high degree of precision.

Convergence and Divergence of PN Axons

A common strategy used for odor coding from insects to mammals is that single odorants activate multiple ORNs and therefore multiple glomeruli; conversely, multiple odorants can activate any single glomerulus (Friedrich and Korsching, 1997; Galizia et al., 1999; Malnic et al., 1999; de Bruyne et al., 2001). Thus, it is the unique combination of activation of a set of glomeruli—a combinatorial code—that defines a given odor. How does the brain integrate the information of simultaneous activation of multiple receptors/glomeruli and perceive it as a single odor? How does the brain distinguish two odors that activate overlapping sets of glomeruli? Anatomically, integration could be achieved by the convergence and divergence of axon projections—single higher-order neurons receiving input from multiple lower-order neurons carrying different olfactory information and single PN classes sending output to multiple third-order neurons.

The nature of the PN axon map in the lateral horn described in our study affords such a possibility. Compared to the glomerular map, in which individual classes of ORNs project their axons to discrete units, the glomeruli, the PN axon map is much more diffuse (Figures 7C–7F). Although members of each glomerular class of PN retain their characteristic branching pattern and terminal fields, the terminal fields of different glomerular classes exhibit considerable overlap. These areas of overlap are also stereotyped, such that third-order neurons that project their dendrites to a particular region of the lateral horn could consistently be activated by a specific set of PNs. One can thus envision a reconstruction procedure in which each PN class connects to a stereotyped set of third-order neurons (see below), and each third-order neuron in turn receives input from a stereotyped set of PN classes.

The degree of convergence would be a function of the dendritic fields of individual lateral horn output neurons, about whose anatomical organization in insects we have virtually no knowledge at present (N. Strausfeld, personal communications). Future genetic tracing experiments analogous to this study on candidate lateral horn output neurons will shed light on this issue.

Most anatomical integration of different olfactory information likely happens at the third-order neuron and beyond. There is, however, at least one vPN that projects its dendrites diffusely throughout the entire antennal lobe, contacting the vast majority of glomeruli, thus providing an extreme case for convergence at the level of the antennal lobe. Interestingly, the axon of this vPN is unique in projecting beyond the lateral horn. What could the function of this vPN be? It is possible that it serves to inform the flies of high odor intensity in the environment without specifically conveying information about a particular odor. It may have a high activation threshold so that only the simultaneous activation of several odorant receptors can stimulate its activity. The relatively low density of dendritic arborization within each glomerulus compared to that of uniglomerular PNs (see Figure 2C$_0$) is consistent with this hypothesis.

Concomitant with convergent projections, PN axons also exhibit divergent projections. In theory, divergent projections could be achieved by two distinct cellular mechanisms. It is possible that second-order neurons that send dendrites to one particular glomerulus have several distinct subclasses, each sending axon projections to one unique higher olfactory center or to different target cells within the same higher center. Alternatively, all second-order neurons corresponding to one particular glomerulus class are homogenous, each one achieving divergent projections by sending stereotypical axon branches to multiple higher-order centers. We found two examples for the first mechanism of divergent projection in our study. Glomeruli DA1 and VA1lm are represented by both vPNs and adPNs or lPNs. Thus, these PNs should carry similar olfactory information. However, DA1(v) and DAl(l) or VA1lm(v) and VA1lm(ad) classes of PNs have distinct branching patterns and terminate at different locations in their common target, the lateral horn (Figure 4).

However, the predominant mechanism used by PNs to achieve divergent projections is through stereotypical axon branching of each individual PN belonging to the same class. Within the lateral horn, several classes of PNs (e.g., DL1, DM6) form stereotypical branches at defined locations, clearly innervating two distinct regions of the lateral horn. Even the local branching patterns of many classes of PNs are strikingly stereotypical (Figures 3 and 4). Moreover, at a gross level, all adPNs and lPNs innervate both the mushroom body and the lateral horn by sending collaterals to mushroom body calyx, thus creating two separate representations in two distinct higher olfactory centers.

How generally applicable are the rules we describe here to other organisms? Recent transneuronal tracing of the central pathways of two divergent ORN classes

in mice revealed stereotypical connections with spatially distinct third order neurons in the olfactory cortex, supporting the notion that the olfactory cortex is spatially organized with regard to the odorant information received (Zou et al., 2001). Moreover, mitral cells that are transneuronally labeled by each ORN class appear to terminate in several different higher olfactory centers. Within a given center, the number of labeled higher-order neurons was much greater than the 1/1000 that would be expected if each third-order neuron received the same number of nonoverlapping inputs (Zou et al., 2001). Thus the stereotypy, divergence, and convergence of the axon projections of the second-order neurons are likely to be conserved features from insect to mammals. It remains to be determined whether other features we described (for example, the correlation between axon projection patterns and glomerular position) are also conserved in mice.

Mushroom Body: A More Plastic Odor Representation?

Much of our analysis has been focused on the axon map in the lateral horn because of the stereotypy of individual PN classes. What about the mushroom body? It has been reported that different odors activated different subsets of *Drosophila* mushroom body intrinsic neurons, suggesting that within individual flies there is spatial segregation of these third-order neurons in their responses to different odors (Wang et al., 2001). Whether this spatial segregation pattern is conserved among different individuals is not known. We found that axon projections in the mushroom body also exhibit a certain degree of stereotypy, as exemplified by the axon projection differences in adPN and lPN neuroblast clones (Figure 2), as well as by the fact that a few mushroom body variables contribute to the discriminant functions (Figure 6C). However, inspection of axon collateral projections of different classes of PNs (Figures 3–5) did not reveal obvious stereotypy as compared to the striking stereotypy of lateral horn axon branching patterns and terminal fields. These observations suggest that the mushroom body dendritic field is organized less stereotypically than that of lateral horn with respect to PN axons.

Perhaps this is not surprising, given what is known about the function of the mushroom bodies. Studies using mushroom body structural mutants, ablation, or learning mutants (e.g., Heisenberg et al., 1985; Nighorn et al., 1991; de Belle and Heisenberg, 1994) indicate that while the mushroom body is essential for olfactory associative learning, it is not essential for odor recognition. By inference, then, the lateral horn must serve the more basic function of odor recognition. Our observations provide anatomical support for this earlier hypothesis: a more stereotypical map in the lateral horn could serve a basic odor recognition function, while a more plastic representation in the mushroom body could contribute to olfactory learning and memory.

Experimental Procedures

Clonal Analysis

MARCM was carried out by heat-shocking larvae of genotype *y w hs-FLP UAS-mCD8-GFP/(+ or Y); FRT^{G13} tubP-GAL80/FRT^{G13} GAL4-GH146 UAS-mCD8-GFP*, and adult and pupal brains were dissected, stained, whole-mounted, and imaged as previously described (Jefferis et al., 2001).

3D Reconstruction

Axon tracing using the software Neurolucida (MicroBrightfield, Colchester, VT) was carried out according to the manufacturer's instructions. Raw confocal images were imported into Neurolucida, and the GFP signal corresponding to the single-cell clone was manually captured. Lateral horn contours revealed by nc82 staining were also traced.

The raw tracing output from Neurolucida was imported into the statistical language R for further processing (http://cran.r-project.org). The first and last branch points of the mushroom body and the first branch point in the lateral horn were manually identified; routines then segmented the axons into main trunk, mushroom body, or lateral horn branches. Further routines then automatically calculated values of the descriptive variables listed below. The program qhull was used to calculate the volumes occupied by the branches (Barber et al., 1996). To compare the spatial locations of neurons in the brain, we scaled the lateral horns of all animals so that the widest points of each lateral horn in the *x*, *y*, and *z* dimensions of our confocal stacks corresponded to ± 1 arbitrary unit. The center was defined as the midpoint in the *z* (anteroposterior) axis and the centroid in the *x* and *y* axes. We were then able to superimpose axon projection patterns in all lateral horns onto a single "standard" lateral horn.

Linear Discriminant Analysis of Axonal Projections

Linear discriminant analysis was carried out in R using the lda function of the MASS package (Venables and Ripley, 1994). To get a reliable estimate of the prediction error rate, which is stated $\pm$SEM, 5-fold crossvalidation (4/5 of the data is used to train, 1/5 to test) was carried out 40 times.

We used an empirical method to determine the relative contribution of these selected variables to the discrimination process. Each variable was removed from the data set in turn, and a 5-fold crossvalidation error rate was calculated as above. The difference between this error rate and the error rate when all variables were present in the data set then indicated the relative "importance" of the variable in question.

Description of Variables

Definitions of variables are listed in the legend to Figure 6. For descriptions of the remaining variables not used in the final discriminant analysis described above, please see Supplementary Data at http://www.cell.com/cgi/contenct/full/109/2/243/DC1.

Permutation Test of Spatial Location in the Lateral Horn

We first derived the mean positions (centroid) in the lateral horn of every neuron's axon endpoints. We then calculated a *dispersion index* to measure the degree to which these mean axon endpoints are clustered by PN class. First, we found the group centroid for all the 13–16 mean axon endpoint positions of a particular PN class; the distances from each mean axon end point position to this group centroid will be small if the mean endpoints are located in a similar spatial position. This calculation was repeated for neurons in all 11 classes to obtain 161 distances that were averaged to give a dispersion index. This dispersion index was 0.23 units in the arbitrary dimensions of our scaled lateral horn (which spans from -1 to $+1$ arbitrary unit), or about 1/8 of the width of the lateral horn. In order to compare this clustering with what might occur by chance if different PN classes did not have stereotypical termination sites, we carried out a permutation test. The PN class of every neuron was swapped with that of another neuron picked at random so that all 161 were randomly relabeled. The mean dispersion index calculated for 2000 such permutations was 0.473 ± 0.0001 units (Figure 7B). In short, no permutation even remotely exhibited the same degree of spatial order as the actual data.

Spatial Relationships of Axon Terminal Fields

We used a nearest neighbor method to do pairwise comparisons of the location of all axon endpoints in the lateral horn for different

PN classes. We extracted all the endpoints for the two classes under consideration, which we now refer to as A and B. For each A endpoint we calculated the proportion of its ten nearest neighbors that were also class A; this proportion was then divided by the proportion of all axon endpoints that were class A. We then took the mean of all these ratios. The same procedure was repeated for points of class B, to give a second mean. The grand mean of these two means was then calculated and one subtracted from this value, to give the final "overlap" score for the pair of glomeruli being tested; a distance of zero would thus correspond to identically distributed axon terminal fields. The matrix of pairwise overlap scores was then used as a distance matrix to construct a dendrogram using Ward's method.

Acknowledgments

We are grateful to Richard Axel for communicating results prior to publication and to Reinhard Stocker and Eric Buchner for reagents. We thank Eric Knudsen, Susan McConnell, Reinhard Stocker, Lubert Stryer, and Fan Wang for comments on the manuscript. E.C.M. and G.S.X.E.J. are Howard Hughes Medical Institute predoctoral fellows. This work was supported by National Institutes of Health grants and a Terman Fellowship to L.L.

Received: December 18, 2001
Revised: March 4, 2002

References

Axel, R. (1995). The molecular logic of smell. Sci. Am. *273*, 154–159.

Barber, C.B., Dobkin, D.P., and Huhdanpaa, H. (1996). The Quickhull algorithm for convex hulls. ACM Trans. Math. Software *22*, 469–483.

Belluscio, L., and Katz, L.C. (2001). Symmetry, stereotypy, and topography of odorant representations in mouse olfactory bulbs. J. Neurosci. *21*, 2113–2122.

Chess, A., Simon, I., Cedar, H., and Axel, R. (1994). Allelic inactivation regulates olfactory receptor gene expression. Cell *78*, 823–834.

Clyne, P.J., Warr, C.G., Freeman, M.R., Lessing, D., Kim, J., and Carlson, J.R. (1999). A novel family of divergent seven-transmembrane proteins: candidate odorant receptors in *Drosophila*. Neuron *22*, 327–338.

de Belle, J.S., and Heisenberg, M. (1994). Associative odor learning in *Drosophila* abolished by chemical ablation of mushroom bodies. Science *263*, 692–695.

de Bruyne, M., Foster, K., and Carlson, J.R. (2001). Odor coding in the *Drosophila* antenna. Neuron *30*, 537–552.

Friedrich, R.W., and Korsching, S.I. (1997). Combinatorial and chemotopic odorant coding in the zebrafish olfactory bulb visualized by optical imaging. Neuron *18*, 737–752.

Galizia, C.G., Sachse, S., Rapert, A., and Menzel, R. (1999). The glomerular code for odor representation is species specific in the honeybee *Apis mellifera*. Nat. Neurosci. *2*, 473–478.

Gao, Q., Yuan, B., and Chess, A. (2000). Convergent projections of Drosophila olfactory neurons to specific glomeruli in the antennal lobe. Nat. Neurosci. *3*, 780–785.

Heisenberg, M., Borst, A., Wagner, S., and Byers, D. (1985). *Drosophila* mushroom body mutants are deficient in olfactory learning. J. Neurogenet. *2*, 1–30.

Hildebrand, J.G., and Shepherd, G.M. (1997). Mechanisms of olfactory discrimination: converging evidence for common principles across phyla. Annu. Rev. Neurosci. *20*, 595–631.

Homberg, U., Mantague, R.A., and Hildebrand, J.G. (1989). Anatomy of antenno-cerebral pathways in the brain of the sphinx moth *Manduca sexta*. Cell Tissue Res. *254*, 255–281.

Hubel, D.H., and Wiesel, T.N. (1962). Receptive fields, binocular interaction and functional architecture in the cat's visual cortex. J. Physiol. (Lond.) *160*, 106–154.

Jefferis, G.S.X.E., Marin, E.C., Stocker, R.F., and Luo, L. (2001). Target neuron prespecification in the olfactory map of *Drosophila*. Nature *414*, 204–208.

Jefferis, G.S.X.E., Marin, E.C., Watts, R., and Luo, L. (2002). Development of neuronal connectivity in *Drosophila* antennal lobes and mushroom bodies. Curr. Opin. Neurobiol. *12*, 80–86.

Jhaveri, D., Sen, A., and Rodrigues, V. (2000). Mechanisms underlying olfactory neuronal connectivity in *Drosophila*-the atonal lineage organizes the periphery while sensory neurons and glia pattern the olfactory lobe. Dev. Biol. *226*, 73–87.

Knudsen, E.I., and Brainard, M.S. (1995). Creating a unified representation of visual and auditory space in the brain. Annu. Rev. Neurosci. *18*, 19–43.

Laissue, P.P., Reiter, C., Hiesinger, P.R., Halter, S., Fischback, K.F., and Stocker, R.F. (1999). Three-dimensional reconstruction of the antennal lobe in *Drosophila melanogaster*. J. Comp. Neurol. *405*, 543–552.

Laurent, G., Stopfer, M., Friedrich, R.W., Rabinovich, M.I., Volkovskii, A., and Abarbanel, H.D. (2001). Odor encoding as an active, dynamical process: experiments, computation, and theory. Annu. Rev. Neurosci. *24*, 263–297.

Lee, T., and Luo, L. (1999). Mosaic analysis with a repressible cell marker for studies of gene function in neuronal morphogenesis. Neuron *22*, 451–461.

Malnic, B., Hirono, J., Sato, T., and Buck, L.B. (1999). Combinatorial receptor codes for odors. Cell *96*, 713–723.

Malun, D., Waldow, U., Kraus, D., and Boeckh, J. (1993). Connections between the deutocerebrum and the protocerebrum, and neuroanatomy of several classes of deutocerebral projection neurons in the brain of male *Periphlaneta americana*. J. Comp. Neurol. *329*, 143–162.

Meister, M., and Bonhoeffer, T. (2001). Tuning and topography in an odor map on the rat olfactory bulb. J. Neurosci. *21*, 1351–1360.

Mombaerts, P., Wang, F., Dulac, C., Chao, S.K., Nemes, A., Mendelsohn, M., Edmondson, J., and Axel, R. (1996). Visualizing an olfactory sensory map. Cell *87*, 675–686.

Nighorn, A., Healy, M.J., and Davis, R.L. (1991). The cyclic AMP phosphodiesterase encoded by the *Drosophila dunce* gene is concentrated in the mushroom body neuropil. Neuron *6*, 455–467.

Penfield, W., and Rasmussen, T. (1950). The Cerebral Cortex of Man: A Clinical Study of Localization of Function (New York: Macmillan).

Ressler, K.J., Sullivan, S.L., and Buck, L.B. (1993). A zonal organization of odorant receptor gene expression in the olfactory epithelium. Cell *73*, 597–609.

Ressler, K.J., Sullivan, S.L., and Buck, L.B. (1994). Information coding in the olfactory system: evidence for a stereotyped and highly organized epitope map in the olfactory bulb. Cell *79*, 1245–1255.

Rodrigues, V. (1988). Spatial coding of olfactory information in the antennal lobe of *Drosophila melanogaster*. Brain Res. *453*, 299–307.

Rubin, B.D., and Katz, L.C. (1999). Optical imaging of odorant representations in the mammalian olfactory bulb. Neuron *23*, 499–511.

Sachse, S., Rappert, A., and Galizia, C.G. (1999). The spatial representation of chemical structures in the antennal lobe of honeybees: steps towards the olfactory code. Eur. J. Neurosci. *11*, 3970–3982.

Stocker, R.F. (1994). The organization of the chemosensory system in *Drosophila melanogaster*: a review. Cell Tissue Res. *275*, 3–26.

Stocker, R.F., Lienhard, M.C., Borst, A., and Fischbach, K.-F. (1990). Neuronal architecture of the antennal lobe in *Drosophila melanogaster*. Cell Tissue Res. *262*, 9–34.

Stocker, R.F., Heimbeck, G., Gendre, N., and de Belle, J.S. (1997). Neuroblast ablation in *Drosophila* P[GAL4] lines reveals origins of olfactory interneurons. J. Neurobiol. *32*, 443–452.

Tsuboi, A., Yoshihara, S., Yamazaki, N., Kasai, H., Asai-Tsuboi, H., Komatsu, M., Serizawa, S., Ishii, T., Matsuda, Y., Nagawa, F., and Sakano, H. (1999). Olfactory neurons expressing closely linked and homologous odorant receptor genes tend to project their axons to neighboring glomeruli on the olfactory bulb. J. Neurosci. *19*, 8409–8418.

Uchida, N., Takahashi, Y.K., Tanifuji, M., and Mori, K. (2000). Odor maps in the mammalian olfactory bulb: domain organization and odorant structural features. Nat. Neurosci. *3*, 1035–1043.

Vassar, R., Ngai, J., and Axel, R. (1993). Spatial segregation of odorant receptor expression in the mammalian olfactory epithelium. Cell *74*, 309–318.

Vassar, R., Chao, S.K., Sitcheran, R., Nunez, J.M., Vosshall, L.B., and Axel, R. (1994). Topographic organization of sensory projections to the olfactory bulb. Cell *79*, 981–991.

Venables, W.N., and Ripley, B.D. (1994). Modern Applied Statistics with S-Plus (New York: Springer-Verlag).

Vosshall, L.B., Amrein, H., Morozov, P.S., Rzhetsky, A., and Axel, R. (1999). A spatial map of olfactory receptor expression in the Drosophila antenna. Cell *96*, 725–736.

Vosshall, L.B., Wong, A.M., and Axel, R. (2000). An olfactory sensory map in the fly brain. Cell *102*, 147–159.

Wang, F., Nemes, A., Mendelsohn, M., and Axel, R. (1998). Odorant receptors govern the formation of a precise topographic map. Cell *93*, 47–60.

Wang, Y., Wright, N.J., Guo, H., Xie, Z., Svoboda, K., Malinow, R., Smith, D.P., and Zhong, Y. (2001). Genetic manipulation of the odor-evoked distributed neural activity in the *Drosophila* mushroom body. Neuron *29*, 267–276.

Wong, A.M., Wang, J.W., and Axel, R. (2002). Spatial representation of the glomerular map in the *Drosophila* protocerebrum. Cell *109*, this issue, 229–241.

Zou, Z., Horowitz, L.F., Montmayeur, J.-P., Snapper, S., and Buck, L.B. (2001). Genetic tracing reveals a stereotyped sensory map in the olfactory cortex. Nature *414*, 173–179.